Evaluating Liquefaction-Induced Lateral Deformation of Earth Slopes using Computational Fluid Dynamics (CFD)

Yaser Jafarian
Department of Civil Engineering, Semnan University, Semnan, Iran.

Ali Ghorbani
Faculty of Engineering, Guilan University, Rasht, Iran.

Omid Ahmadi
International Branch, Guilan University, Rasht, Iran.

SUMMARY:
Liquefiable soils within earth slopes are prone to lateral deformation, which is a cause of significant damage in earthquakes. In the recent decade, researchers have presented studies in which liquefied soils is considered as viscous fluid. In such manner, the liquefied soil behaves as non-Newtonian fluid, whose viscosity decreases with increasing shear strain rate. The current study uses computational fluid dynamic to predict liquefaction-induced lateral deformation of an infinite earth slope. Post-liquefaction residual strength of soil is incorporated to estimate Bingham viscosity within an Incremental Elastic Model. An iterative scheme is presented to estimate strain-compatible soil stiffness. Centrifuge model tests are numerically simulated in this study to validate the numerical simulation. The results, which are considered in terms of the displacements of the liquefied soil masses, confirm that the computed and the measured soil displacements are in agreement within a reasonable degree of precision.

Keywords: liquefaction, lateral spreading, computational fluid dynamics

1.INTRODUCTION

Liquefaction of loose and saturated soil deposits has produced catastrophic failures during the earthquakes. This phenomenon produces disastrous consequences such as lateral spreading in free-face and gently sloping grounds. Liquefaction-induced lateral spreading has caused massive damages to deep foundation of buildings and bridges, embankments and lifeline systems. During the 1964 Niigata earthquake, lateral movement of liquefied soils resulted in considerable bending and failure of pile systems. In the same year, wide spread lateral ground deformations were observed for more than 250 bridges and embankments along the Alaskan railroads and highways.
Several methods have been presented in the literature to predict the displacements produced by liquefaction-induced lateral spreading. They can be classified into the following groups: (1) empirical, (2) numerical, and (3) simplified analytical methods. Researchers have carried out numerical study to simulate behavior of liquefied soil as a reduced-stiffness solid. Based on this assumption, Yasuda et al. (1992) proposed a simple static finite element analysis in two stages to assess the lateral spreading. In this approach, the stress regime in the ground is calculated using the elastic modulus before shaking starts and then the stresses are held constant and analysis is conducted again using the shear modulus decreased due to liquefaction. By the principle of minimum potential energy, Towhata and Orense (1992) proposed a three dimensional finite element approach to predict the permanent displacements. By assuming the liquefied soil as a visco-elastic material, Aydan (1995) proposed a finite element approach based on an adaptive mesh technique. Moreover, Uzouka et al. (1998) developed a numerical method to predict lateral spreading of liquefied soil based on fluid dynamics. They used a numerical method by assuming liquefied soil as a Bingham fluid. Hadush et al. (2001) employed cubic

interpolated pseudo-particle, CIP-based numerical scheme, by incorporating the Bingham viscosity to estimate the lateral displacement.

Literature survey reveals that variety of numerical methods has been developed to predict lateral spreading by treating the liquefied soil as solid or viscous fluid. Some of these approaches such as Iai (1989), Hamada (1998), and Wakamatsu (1998) assumed that deformation is regarded as small, less than 10%, while this assumption cannot be applied to lateral spreading.

This paper treats liquefied soil as fluid using the Bingham model, incorporating incremental elastic stress model in the framework of fluid dynamic. The liquefaction–induced lateral spreading is predicted from non-Newtonian flow analysis using FLOW-3D code that is one of the desirable computational fluid dynamics (CFD) programs for simulating flow problems. Computational fluid dynamic is a method of flow simulation in which standard flow equations such as Navier-Stokes and continuity equation are discretized and solved for each computational cell. FLOW-3D numerically solves the equations described above using finite difference (or finite volume). To determine viscosity and yield stress of the liquefied soil, the Bingham model which incorporates incremental elastic stress model was used. A centrifuge model test is simulated herein to predict lateral deformations of its laminar box which were monitored by LDVTs. An iterative numerical scheme was developed to calculate the strain-compatible shear modulus of the liquefied soil along the height of the simulated soil. Results of the numerical simulation have shown to be in accord with the measurements at the superficial soils, wherein displacement prediction is important, while over-estimated displacements are obtained at deeper zones.

2. THEORETICAL BACKGROUND

2.1.Incremental Elastic Stress Model

FLOW-3D code employs incremental elastic stress model to emulate visco-plastic materials such as Bingham materials which behave as a solid until reaching a certain yield stress. Beyond the yield stress, they behave like a viscous fluid. The state of stress for a Newtonian viscous fluid is:

$$\mathbf{T}=2\mu\dot{\boldsymbol{E}} \qquad (2.1)$$

where μ is the viscosity coefficient, $\dot{\boldsymbol{E}}$ is the strain rate tensor, and **T** is the Cauchy stress tensor. In contrast, the stress state for a Hookean elastic solid is:

$$\mathbf{T}=2\mathbf{GE} \qquad (2.2)$$

where **G** and **E** are elastic modulus and strain tensor, respectively. Figure 1 illustrates a schematic simplification of a visco-plastic model.

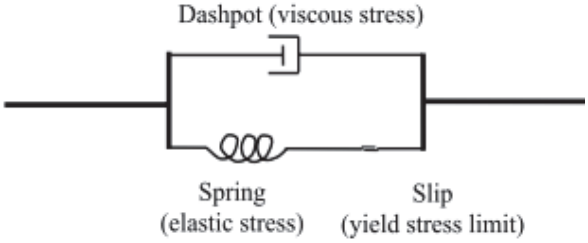

Figure 1. Pictorial view of visco-plastic model

A visco-plastic model predicts a corresponding rise in elastic stress that is linearly proportional to the strain. If further strain be imposed to a point such that the elastic stress exceeds the yield stress, the material yields and begins to flow as a viscous fluid with an equivalent viscosity.

This study uses Bingham model to predict the equivalent viscosity once elastic stress exceeds the yield stress. In the next section, the Bingham plastic is described to predict lateral deformation of

liquefied soils. The employed code utilizes a fixed-mesh Eularian approach to compute the elastic stresses. For an element of fluid, the elastic stress description is:

$$\boldsymbol{\tau_E(\varepsilon, t) = \int_{-\infty}^{t} 2G\,\dot{E}(\varepsilon, t')dt'} \qquad (2.3)$$

where τ_E is the elastic stress tensor and ε is material coordinate which represent the deformation of material. $\dot{E}$ is the local strain rate tensor:

$$\boldsymbol{\dot{E} = \frac{1}{2}[\nabla_u + (\nabla_u)^T]} \qquad (2.4)$$

u is the local velocity vector. The time rate of change for Eq. 2.3 is:

$$\boldsymbol{(\frac{\partial_{\tau_E}}{\partial_t})_x + u.\,\nabla_{\tau_E} = 2G\dot{E}(X, t)} \qquad (2.5)$$

where τ_E stands for the elastic stress tensor represented in fixed coordinate system (Eulerian approach), which corresponds to the mesh used in FLOW-3D. The Mises yield condition is assumed as:

$$\boldsymbol{\prod_{\tau_E} = \frac{Y^2}{3}} \qquad (2.6)$$

where Π_{τ_E} is the second invariant of the elastic stress tensor and Y is a yield stress limit. If there is a region in material where the elastic stress exceeds the yield criterion, the elastic stress is relaxed by:

$$\boldsymbol{\tau_E^* = \sqrt{\frac{2Y^2}{3\prod_{\tau_E}}}\tau_E} \qquad (2.7)$$

where τ_E^* is the yield limited elastic stress tensor. Eq. 2.5 is spatially discretized and the resulting elastic stress is added into the momentum equation as:

$$\boldsymbol{\frac{\partial_u}{\partial_t} + u.\nabla u = -\frac{1}{\rho}\nabla p + \frac{1}{\rho}\{\nabla.\left[\mu\left(\nabla u + (\nabla u)^T\right)\right] + F_B + \nabla.\tau_E^*\}} \qquad (2.8)$$

The last term in this equation is divergence of elastic stress tensor.

Bingham Model

The Bingham model was employed to simulate the behavior of liquefied soil once the yield stress is surpassed. In order to predict the viscous stress, the Bingham fluid, which is a visco-plastic model considering the residual strength, is implemented. Uzuoka et al. (1998) confirmed that the Bingham model is applicable to the behavior of liquefied soil. They assumed the equivalent coefficient by the following equation:

$$\boldsymbol{\mu' = \mu + \frac{\tau_r}{2\dot{\gamma}}} \qquad (2.9)$$

in which,

$$\boldsymbol{\dot{\gamma} = \sqrt{(\frac{1}{2})e_{ij}e_{ij}}} \qquad (2.10)$$

where $\dot{\gamma}$ is second invariant of strain rate tensor or the effective strain rate. The components of the strain rate tensor are given by

$$e_{ij} = \frac{1}{2}\left[\frac{\partial u_i}{\partial x_j} + \frac{\partial u_j}{\partial x_i}\right] \quad (2.11)$$

and τ_r is the yield stress (minimum undrained strength). The residual strength of soil is taken into account to determine the minimum undrained strength, as discussed in the following section. The minimum undrained strength has an important role and has been used to indicate whether flow occurs.

3.Residual Strength

In this study, the residual strength of soil is considered to estimate the yield stress in Bingham model and to determine the equation of equivalent viscosity of the liquefied soil. Therefore, it is important to have a reasonable estimation of this quantity. Several researchers have presented recommendations for this post-liquefaction parameter. Idriss and Boulanger (2008) have presented two recommendations in the EERI monograph; critical state approach (S_{U_r}) and (S_{U_r}/P). These new recommendations are less conservative than the previous recommendations. Figure 2 shows various recommendations of residual shear strength versus the equivalent clean sand corrected SPT blow counts.

Seed (2010) reviewed Idriss and Boulanger (2008)'s report and indicated serious errors in plotting of these data. In fact, the former professor Seed (Seed 1987) had made an error in back-calculation of S_{U_r} values for field performance cases in which liquefaction induced displacements had been large; resulting in considerable over-estimation of S_{U_r} for those cases. Seed (2010) recommended the following procedure to estimate the post-liquefaction residual strengths. The heavy dashed line in Figure 2(b) is the best current set of recommendations based on critical state approach. The most valid explanation of the field data within the alternative S_{U_r}/P based approach would be obtained using the heavy dashed line in Figure 2(a).

(a) (b)

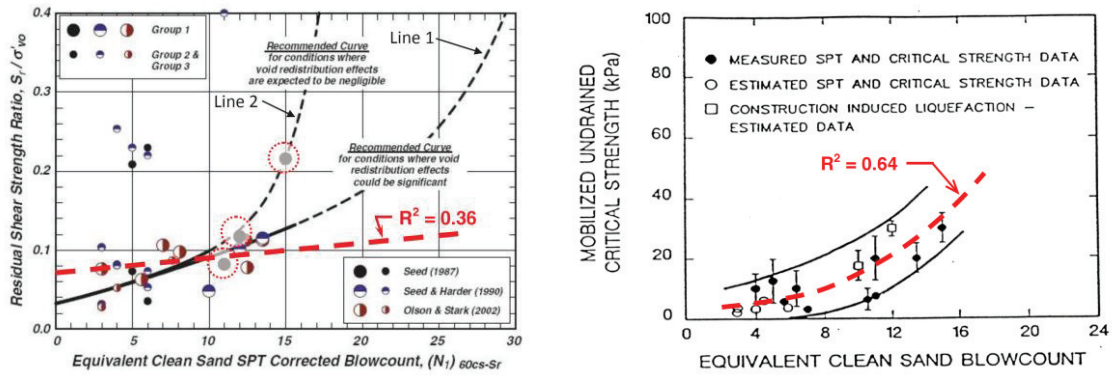

Figure 2. (a) Recommendations of Seed (2010) based on the interpretations of Idriss and Boulanger (2008), (b) Residual strength as a function of equivalent SPT blow counts (after Seed and Harder 1990 and Seed 2010)

4.Shear modulus of incremental elastic stress model

In the previous sections, the incremental elastic stress model was explained and method of estimating elastic stress distribution was demonstrated. For this method of fluid dynamics, one has to estimate the shear modulus of the liquefied soil as the representative parameter of soil behavior during liquefaction. It is known that shear modulus of granular soils reduces during undrained cyclic loading up to liquefaction onset. Mean shear modulus of soil was taken into account as the identical parameter of the whole liquefaction procedure. To take this mean shear modulus into the simulation, the G/G_0 reduction curves are implemented in the analysis, which are commonly employed in the well-known

equivalent linear approximation of nonlinear response. Figure 3 shows the G-reduction (G/G0) curve proposed by Seed and Idriss (1970), which was used in the current study.

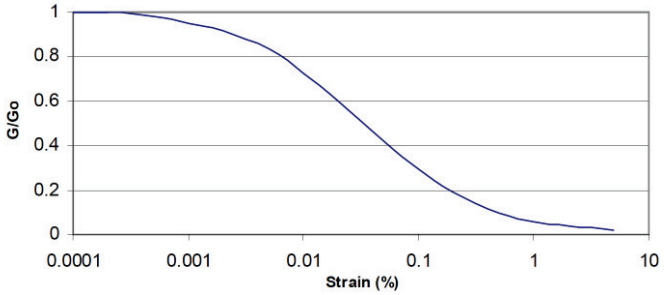

Figure 3. Average shear modulus reduction curve for sand (after Seed and Idriss, 1970)

Effective shear modulus is generated by normalizing the shear strain history within any given depth of soil layer using the displacement data and shear strain equation. For small displacement gradients and small rotation, the shear strain equation is:

$$\gamma_{xy} = \frac{\partial_{dy}}{\partial_x} + \frac{\partial_{dx}}{\partial_y} \quad (4.1)$$

For the analysis with unknown displacement history, equivalent linear approximation is applicable. In this approach, it is common to gain the strain level of seismic loading in term of an effective strain which has been found to vary between 50 to 70% of the maximum shear strain. Here, the effective strain in each step can be predicted by this equation:

$$\gamma_{eff} = .65\gamma_{max} \quad (4.2)$$

where γ_{max} is maximum shear strain at the depth under consideration.

5.CENTRIFUGE EXPERIMENT

The lateral spreading experiment in the inclined soil container of a centrifuge model test conducted during VELACS project is simulated herein. . The centrifuge VELACS model No. 2, which was conducted by Dobry and Taboada (1994), simulates a mildly inclined infinite slope with effective inclination angel of about 4°. Figure 4a shows the laminar container of this experiment and arrangement of the instruments. Also, Figure 5b illustrates time history of input acceleration. Table 5.1 presents the basic soil properties of Nevada sand which was used in the mentioned experiment.

Table 5.1. Soil properties in the centrifuge model test (Taboada 1995)

Soil	Density	D_r	e_{max}	e_{min}
Nevada sand	1962 kg/m^3	40%	0.887	0.511

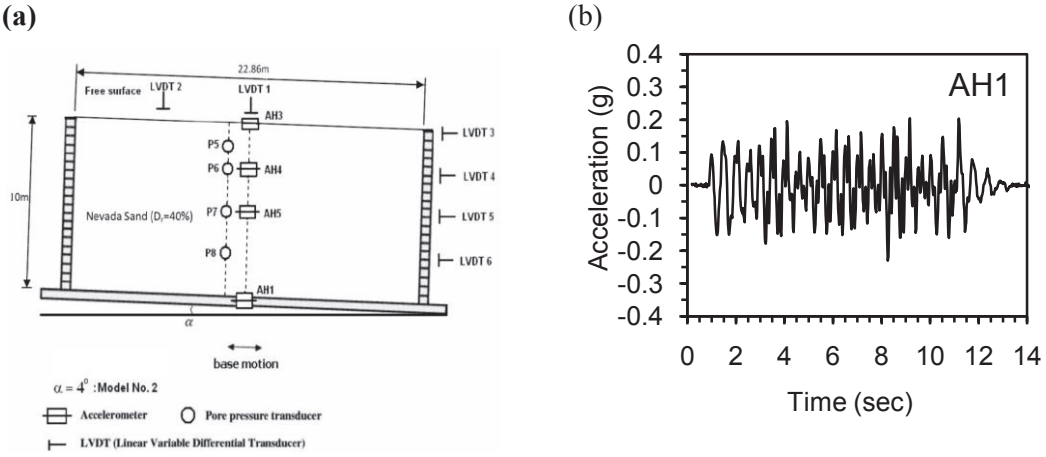

Figure 4. (a) Illustration of VELACS centrifuge Model No.2, (b) Base acceleration in the centrifuge test

6.NUMERICAL MODELING PROCEDURE

The centrifuge tests were simulated using the described models in FLOW-3D. To simulate the free surface condition at the top of the container, the specific pressure boundary with zero fluid volume fraction ratios was utilized and non-slip wall boundary was specified for the other boundaries. The AH1 acceleration time history (shown in Figure 4b) was introduced as base acceleration to the base of the simulated container in non-inertial reference frame.

Determination of the analytical parameters of Bingham viscosity and incremental elastic stress was explained in the preceding sections. For the VELACS model No. 2, the following equation, which was proposed by Cubrinovski and Ishihara (1999), was employed to correlate relative density and SPT blow counts for the estimation of residual strength from the previously shown graphs .

$$\frac{(\mathbf{N_1})_{60}}{\mathbf{D_r}^2} = \frac{\mathbf{11.7}}{(\mathbf{e_{max} - e_{min}})^{1.7}} \qquad (\mathbf{6.1})$$

For Nevada sand with $D_r = 40\,\%$ and maximum and minimum void ratios cited in Table 1, SPT blow counts of about ≈ 10 is resulted in. Consequently, the residual strength in each approach can be easily derived from Figures 2 (a and b). Table 6.2 presents the residual strength according to Seed (2010)'s recommendation. The quantities were determined in the middle of soil layer as the representative of the whole layer.

Table 6.1. Estimation of residual strengths from various recommendations

$(N_1)_{60}$	(FC)%	$(N_1)_{60-CS}$	**residual strength kPa**
9.87	7	11	7.5

By employing the weighted residual strength, the Bingham viscosity parameter can be found by the following equation once stresses tend to exceed the yield stress:

$$\boldsymbol{\mu}' = \boldsymbol{\mu} + \frac{\boldsymbol{\tau_r}}{\mathbf{2\dot{\gamma}}} = 695 + \frac{\mathbf{3750}}{\dot{\boldsymbol{\gamma}}} \qquad (6.2)$$

For incremental elastic stress, it is required to specify the shear modulus, G, and yield stress. The residual strength of 7.5 kPa is considered as the yield stress. To drive the shear modulus, it is required

to predict maximum shear modulus G_0 to assign the $\frac{G}{G_0}$ in equivalent linear approximation of shear modulus. Several researchers have been proposed a number of empirical equations as form of Eq. (6.3) by various constants to determine the small-strain shear stiffness of soil.

$$G_0 = A.F(e)(\acute{\sigma_0})^n \tag{6.3}$$

Table 6.2. Constants proposed for empirical equations (Kokusho, 1987)

References	A	F(e)	n
Hardin-Richart (1963)	7000	$\frac{(2.17-e)^2}{(1+e)}$	.5
Hardin-Richart(2) (1963)	3300	$\frac{(2.97-e)^2}{(1+e)}$	.5
Iwasaki et al.(1978)	9000	$\frac{(2.17-e)^2}{(1+e)}$	.38
Kokusho (1980)	8400	$\frac{(2.17-e)^2}{(1+e)}$	.5

An iterative operation has been utilized by assuming an initial G at small strain levels and using the estimated G to compute the response including the time histories of shear strain for any given layer. To determine the effective shear strain, Eq. 13 along with the G-reduction curve were repeatedly used for estimating new equivalent linear G^{i+1} for the next iteration. These steps are repeated until differences between computed shear modulus in two successive iterations fall below a prescribed value.

7. SIMULATION RESULTS AND DISCUSSION

7.1. Time history of ground displacement

Figures 5 (a to d) compare simulated and measured lateral displacements in the VELACS centrifuge model No. 2. As seen, the triggering points of lateral displacement roughly agree with the experimental results shown in Figure 5. Furthermore, the predicted displacements in the middle and top of the layer have acceptable trend compared with the measured values of lateral displacements. In the deeper levels, however, the model overestimates the displacements. Inaccurate predictions in deep zones can be related to high equivalent viscosity in the lower levels of soil layer with the small shear strain rate happened due to the use of constant value of minimum undrained shear strength along the height. Similar observation was reported by Mounir (2006) for the deeper depths of the shaking table tests simulated by computational fluid dynamics.

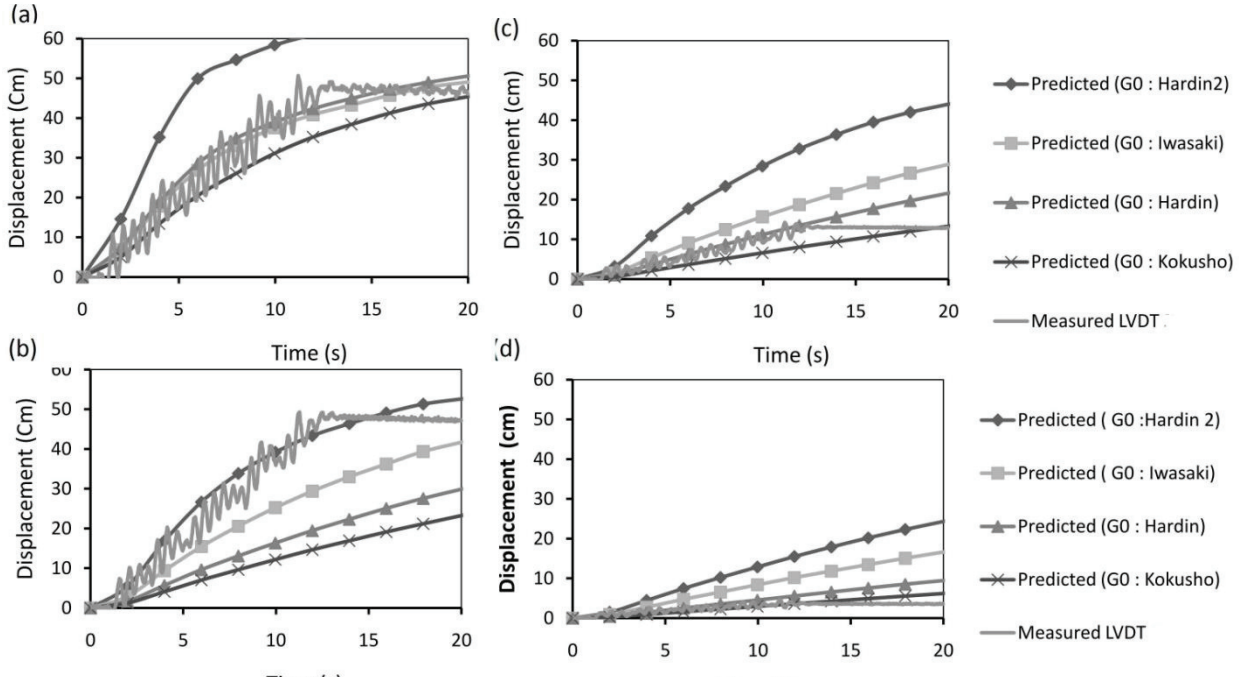

Figure 5. Comparison between the simulated and measured values of lateral displacements in the LVDTs level (a) LVDT3, (b) LVDT4, (c) LVDT5, (d) LVDT6

7.2 SUMMARY AND CONCLUSION:

This paper presented a finite difference-volume fluid dynamic method to predict the liquefaction induced lateral spreading of liquefiable soils using Bingham model. Post-liquefaction shear modulus and residual strength were considered in the model to estimate the shear stress and equivalent viscosity. The numerical model was applied to a centrifuge model test simulating a mildly sloping sand deposit. The results show that the predicted lateral displacements at the top section of soil layer agree with the experimental results. At the bottom of soil layer, the results are over-estimated because of the small shear strain rate considered for the bottom sections. The iterative procedure, which was used in this numerical study, obtains compatible shear strains that are in agreement with those achieved by the back analysis of the centrifuge experiment.

REFERENCES

Aydan, O. (1995). Mechanical and numerical modeling of lateral spreading of liquefied soil. *Proc.1st Int Conf on Earth-Geo Eng*, Tokyo 881-886.

Brethour, J. M. (2003). Incremental elastic stress model. Flow Science, Inc FSI-03-TN64.

Cubrinovski, M. and Ishihara, K. (1999). Empirical correlation between SPT N-value and relative density for sandy soils. *Soil and Found*.,**39(5)**; 61-72.

Dobry, R., Taboada, V., Liu, L. (1995). Centrifuge modeling of liquefaction effects during earthquakes, *Proceedings of the first international conference on Earthquake Geotechnical Engineering*. Tokyo, Japan, pp. 1291-324.

Elgamal, A., Yang, Z., Parra, E. (2002). Computational modeling of cyclic mobility and post liquefaction site response. *Soil Dynamics and Earthquake Engineering*, **22**, pp. 259-271.

Flow-3D. (2008). User manual, version 9.3. Flow Science, Inc.

Hadush S., Yashima A., Uzuoka R. (2000). Importance of viscous fluid characteristics in liquefaction induced lateral spreading analysis. *Computers and Geotechnics* **27**, pp. 199-224

Hadush S., Yashima A., Uzuoka R., Moriguchi S. Sawada K. (2001).Liquefaction induced lateral spread analysis using the CIP method. *Computer and Geotechnics* **28**, pp. 549-574.

Hamada M, Wakamatsu K. (1998). A study on ground displacement caused by soil liquefaction. *Journal of Geotechnical Engineering*, JSCE; **III-43**(596):189-208.

Hardin B.O., Richart F.E. (1963). Elastic wave velocities in granular soils. *Journal of Soil mechanics and*

Foundations, ASCE, **89**, SM1, 33-65

Hwang J, Kim C, Chung C. K, Kim M. M. (2006). Viscous fluid characteristics of liquefied soils and behavior of piles subjected to flow of liquefied soils. *Soil dynamics and Earthquake Engineering* **26** , 313-323.

Iai S. (1989). Similitude for shaking table tests on soil-structure-fluid model in 1g gravitational field. *Soils and Foundations*; **29**(1):105-18.

Idriss, I.M and Boulanger, R. W. (2008). Soil liquefaction during earthquakes. monograph series, no. MNO-12, Earthquake Engineering Research Institute.

Ishihara K. (1996). Soil Behavior in Earthquake Geotechnics, *Oxford University Press Inc.*

Iwasaki, T., Tatsuoka, F., Tokida, K., and Yasuda, S. (1987). A practical method for assessing soil liquefaction potential based on case studies in various sites in japan. *Proceedings of the 2nd International Conference on Microzonation for Safter Construction-Research and Application.* **Vol. 2**, pp. 85-96

Kokusho, T. (1980). Cyclic triaxial test of dynamic soil properties for wide strain range. *Soils and Foundations,* **20,** 45-60

Kramer S. L. (1996). Geotechnical Earthquake Engineering, *Prentice-Hall*, Inc.

Mounir N. (2006). Analysis of liquefaction induced lateral ground displacement Using Smoothed Particle Hydrodynamics. Ph.D. Dissertation, University of Tsukba, pp. 135.

Olsen P. A. (2008). Shear modulus degradation of liquefying sand: Quantification and Modeling. M.Sc. thesis, Brigham Young University.

Orense, R, Towhata. (1994). Prediction of liquefaction-induced permanent ground displacement: A three dimensional approach.Proc. 4th US-Japan workshop on Earthquake Resistant Design of lifeline Facilities and countermeasures against Soil liquefaction, *Technical report NCEER* **92-0019**, 335-349.

Parra E. (1996). Numerical modeling of liquefaction and lateral ground deformation including cyclic mobility and dilation response in soil system. PhD Thesis, Department of Civil Engineering, Rensselaer Polytechnic Institute, Troy, NY.

Popescu R., Prevost J. H. (1993). Centrifuge validation of a numerical model for dynamic soil liquefaction.*Soil dynamics and earthquake Engineering* 12 73-90.

Schnaid F. (2009). In Situ Testing in Geomechanics, *Taylor and Francis*, first published.

Seed, H.B. (1987). Design problems in soil liquefaction. *Journal of Geotechnical Engineering*, ASCE, **Vol. 113**, No. 8.

Seed, H.B., and Idriss, I.M. (1970). Soil moduli and damping factors of dynamic response analysis. *EERC Rep*. 70-10, University of California, Berkeley, Calif.

Seed R. B. (2010). Technical review and comments: 2008 EERI Monograph, Soil liquefaction during earthquakes. *Geotechnical Report* No**. UCB/GT – 2010/01**. University of California at Berkeley.

Taboada V.M. (1995). Centrifuge modeling of earthquake-induced lateral spreading in sand using a laminar box. PhD Thesis, Rensselaer Polytechnic institute, Troy, NY.

Uzuoka R., Yashima A., Kawakami T., and Konard J.M. (1998). Fluid dynamics based prediction of liquefaction induced lateral spreading. *Computers and Geotechnics***, 22**, **No ¾**, pp 243-282.

Yasuda S., Yoshida N., Masuda T., Nagase H., Mine K., Kiku H., Uchida Y. (1992). The mechanism and simplified procedure for analysis of permanent ground displacement due to liquefaction. *Soils and Foundations*, **32(1)**, 149-160.